A study on MHD flow of SWCNT-Al2O3/water hybrid nanofluid past a vertical permeable cone under the influence of thermal radiation and chemical reactions

Article *in* Numerical Heat Transfer Applications · May 2023

DOI: 10.1080/10407782.2023.2207731

2 authors:


Shiva Rao
Dibrugarh University


P. N. Deka
Dibrugarh University

Numerical Heat Transfer, Part A: Applications
An International Journal of Computation and Methodology

ISSN: (Print) (Online) Journal homepage: https://www.tandfonline.com/loi/unht20

A study on MHD flow of *SWCNT-Al_2O_3*/water hybrid nanofluid past a vertical permeable cone under the influence of thermal radiation and chemical reactions

Shiva Rao & P. N. Deka

To cite this article: Shiva Rao & P. N. Deka (2023): A study on MHD flow of *SWCNT-Al_2O_3*/water hybrid nanofluid past a vertical permeable cone under the influence of thermal radiation and chemical reactions, Numerical Heat Transfer, Part A: Applications, DOI: 10.1080/10407782.2023.2207731

To link to this article: https://doi.org/10.1080/10407782.2023.2207731

Published online: 03 May 2023.

NUMERICAL HEAT TRANSFER, PART A: APPLICATIONS
https://doi.org/10.1080/10407782.2023.2207731

Taylor & Francis
Taylor & Francis Group

Check for updates

A study on MHD flow of *SWCNT-Al_2O_3*/water hybrid nanofluid past a vertical permeable cone under the influence of thermal radiation and chemical reactions

Shiva Rao and P. N. Deka

Department of Mathematics, Dibrugarh University, India

ABSTRACT

This study investigates the steady, incompressible MHD flow of a hybrid nanofluid over a vertical solid cone embedded in a porous medium under suction effect. The research explores the effects of various factors, such as thermal radiation, chemical reactions, heat generation, viscous dissipation, and Joule heating on heat and mass transfer phenomena. To investigate the effects of hybrid nanoparticles, we consider single-walled carbon nanotubes (*SWCNT*) and alumina (*Al_2O_3*) along with water (*H_2O*) as the base fluid. After a suitable similarity transformation, the governing equations are reconstructed and solved using the Keller-box numerical scheme. We present graphical and tabular analyses of various parameter impacts on heat transfer profiles and coefficients. This study provides valuable insights into the control of fluid dynamics and heat transfer in porous media, which have significant implications for industrial and engineering applications. The findings of the current article are in excellent agreement with previously published works.

ARTICLE HISTORY
Received 16 November 2022
Revised 31 March 2023
Accepted 21 April 2023

KEYWORDS
Chemical reactions; hybrid nanofluid; Joule heating; porous medium; suction; thermal radiation; vertical solid cone

1. Introduction

Due to their exceptional ability to transport heat in a variety of engineering and commercial applications, nanofluids have attracted the interest of many researchers. Convectional fluids such as water, ethylene glycol, and engine oil are often poor heat conductors due to their poor thermal conduction, which makes them inefficient in today's modern cooling applications. Nanofluids consist of nanoscale particles such as copper, alumina, carbides, nitrides, metal oxides, graphite, and carbon nanotubes, which enhance the thermal conductivity of base fluids. The diameter of such nanoparticles may vary anywhere between 1 and 100 nm. It was Choi and Eastman [1] who first observed that nanoparticles suspended in base fluid could enhance the thermal conductivity, which in turn improved the heat transfer rate of the fluid. After evaluating the thermal conductivity of various metal oxides, Lee *et al.* [2] found that both shape and size contributed significantly to the improved thermal conductivity of the nanofluid. Later, Buongiorno [3] investigated the factors that influenced the thermal conductivity of nanofluids and reported that Brownian motion and the thermophoresis effect increase the nanofluid's thermal conductivity. As a consequence of the revelation, Nield and Kuznetsov [4] used Buongiorno's model on the boundary layer stream.

Later, Khan and Pop [5] explored the steady flow of nanofluid on a stretching sheet. Using convective boundary conditions, Makinde and Aziz [6] looked into the heat transfer characteristics of nanofluid flow. Khan *et al.* [7] conducted research analyzing the rheological behavior of a nanofluid and investigating the effects of various parameters on its viscosity and other rheological

CONTACT Shiva Rao shivarao374@gmail.com Department of Mathematics, Dibrugarh University, Dibrugarh 786004, India

Nomenclature

a	constant (-)
x, y	Cartesian coordinates along the surface and normal to it, respectively (m)
r	radius of the cone (m)
u, v	velocity component along x-axis and y-axis respectively ($m\ s^{-1}$)
T	temperature (K)
C	nanoparticle concentration ($mol\ L^{-1}$)
B_o	magnetic field (T)
g	gravity due to acceleration ($m\ s^{-2}$)
k_o	porous term (m^2)
Q_o	coefficient of heat generation (Wm^{-3})
C_p	specific heat at constant pressure ($J\ kg^{-1}\ K^{-1}$)
q_r	radiative heat flux (Wm^{-2})
D_m	mass diffusivity ($m^2\ s^{-1}$)
Kr	first order chemical reaction (s^{-1})
k^*	mean absorption co-efficient (m^{-1})
M	magnetic parameter (-)
Gr	Grashof number (-)
Gc	modified Grashof number (-)
Ec	Eckert number (-)
Q	heat generation/absorption (-)
Sc	Schmidt number (-)
K_p	permeability parameter (-)
E_c	Eckert number (-)
Pr	Prandtl number (-)
Rd	radiation parameter (-)
Cf_x	skin-friction coefficient (-)
Nu_x	Nusselt number (-)
Sh_x	Sherwood number (-)
Re_x	Reynold number (-)

Greek Symbols

ν	kinematic viscosity ($m^2 s^{-1}$)
μ	dynamic viscosity ($kg\ m^{-1} s^{-1}$)
σ	electrically conductivity ($S\ m^{-1}$)
ρ	density ($kg\ m^{-3}$)
κ	thermal conductivity of the nanofluid ($W\ m^{-1}\ K^{-1}$)
Ω	angle of the cone (°)
β_t	co-efficient of thermal expansion (K^{-1})
β_c	co-efficient of concentration expansion (C^{-1})
ϕ_1	volume fraction of $SWCNT$ nanoparticles (-)
ϕ_2	volume fraction of Al_2O_3 nanoparticles (-)
σ^*	Stefan-Boltzmann coefficient ($W\ m^{-2}\ K^{-4}$)
η	similarity variable (-)
ψ	stream function ($m^2\ s^{-1}$)
$f\ '$	dimensionless velocity (-)
θ	dimensional temperature (-)
ϕ	dimensionless concentration (-)
γ	chemical reaction parameter (-)

Superscript

$'$	derivative with respect to η

Subscript

w	at wall
∞	at free stream region
hnf	for hybrid nanofluid
nf	for nanofluid with single nanoparticle
f	for base fluid
$s1$	for $SWCNT$ nanoparticles
$s2$	for Al_2O_3 nanoparticles

properties. Hussain and Azeem Khan [8] explored the time-dependent behavior of a polymer nanofluid in the presence of thermal-solutal stratifications and activation energy. Tabrez and Azeem Khan [9] investigated the physical properties of ferromagnetic polymer nanofluids' flow, including viscous dissipation and magnetic dipole. The heat and mass transfer characteristics of a radiative steady and MHD Casson nanofluid flow over a porous stretching sheet are explored by Rao and Deka [10]. The literature cited in Ref. [11–13] includes recent work on nanofluids.

Due to its wide range of potential applications in nanotechnology and medicine, the study of heat transfer in carbon nanofluids has attracted significant attention from researchers in recent years. Nanoparticles of carbon nanotubes (CNTs) were first discovered in 1991 by Iijima [14]. These are allotropes with a nanostructure in the form of a hollow tube composed of a cylindrical framework of carbon atoms, typically has a diameter between 1 and 100 nm. Compared to other nanocomposite forms, CNTs in base fluid are more efficient due to the C-C bond. CNT nanofluid may be manipulated covalently or non-covalently to get the desired result. CNTs have 15 times the thermal conductivity and 1000 times the capability of copper, in addition to 200 times the power and five times the resistance of steel (Prajapati *et al.* [15] and Khalid *et al.* [16]). Significant use of carbon nanotubes may be found in several areas of nanotechnology, including hardware, optics, energy storage, biomedicine, ceramics, thermal defence and engineering (Hayat *et al.* [17]). Due to their small size, structure, configuration, dimension, and hardness, they provide a number of advantages that aren't seen in other nanomaterials. Additionally, the presence of carbon chains in CNTs does not endanger the atmosphere (Alsagri *et al.* [18]). Carbon nanotubes used in nanofluids are divided into two types, called single-walled carbon nanotubes (SWCNTs) and multi-walled carbon nanotubes (MWCNTs), based on how many layers of rolled graphite sheets are in each tube. In contrast to MWCNTs, which may be created without a catalyst and consist of several rolled layers of graphite with a complicated structure, SWCNTs need a catalyst for their synthesis and are prepared by fuzing a covering layer of graphite into a unified cylinder (Khan *et al.* [19]). Kumaresan *et al.* [20] experimentally examined the heat transfer characteristics of nanofluids, including CNTs, and found low nanoparticle volume fractions enhance heat transfer rate. Under the impact of magnetic force and thermal radiation, Mahanthesh *et al.* [21] looked into the energy transport phenomena of dispersing SWCNT and MWCNT in water nanofluids. When compared to MWCNT nanofluid, they found that SWCNT nanofluid had a more even temperature distribution. Some recent advancements on nanofluid using CNT nanoparticles were made by Hossain *et al.* [22], Rehman *et al.* [23], and Maatki *et al.* [24].

A new type of fluid, called a hybrid nanofluid, is finding widespread technological usage due to its excellent thermophysical properties. Hybrid nanofluid is an advanced fluid composed by adding two or more nanoparticles to a base fluid. Such kinds of nanofluids have more advanced properties than conventional nanofluids. An individual substance may never possess all of the needed traits; hence, the substance may be missing or deficient in some properties. Customizable hybrid nanoparticles can process important information more effectively than other nanofluids. Hybrid nanofluids outperform ordinary nanofluids in a variety of heat transfer applications, making them ideal for use in industries as diverse as refrigeration, electronics cooling, drug reduction, generator cooling, machining coolant, cooling for nuclear systems, cooling for transformers, biomedicine, and many more. Sundar [25] has suggested a detailed procedure for creating hybrid nanofluids, including their benefits and drawbacks. Waini *et al.* [26] have studied the unsteady flow of a hybrid nanofluid made by adding Cu nanoparticles in Al_2O_3/water nanofluid due to a stretching/shrinking sheet. Shreedevi *et al.* [27] have mixed both carbon nanotubes and sliver nanoparticles in the base fluid (water) to study the effect of thermal radiation, chemical reaction, suction, and slip condition on the heat and mass transfer of an unsteady MHD flow over a stretching surface. Yashkun *et al.* [28] have investigated the effect of thermal radiation and suction on the dynamics of an MHD hybrid nanofluid as it moves through a stretching/shrinking sheet, particularly emphasizing on the heat transfer. His findings show that the hybrid nanofluid $(Cu - Al_2O_3/water)$ is more efficient than the nanofluid $(Cu/water)$ for the heat transfer phenomena. Recently, Alkasasbeh [29] has investigated the effects of heat transfer and a magnetic field on the flow of a Casson hybrid nanofluid composed by mixing the nanoparticles of copper oxide and graphite oxide in methanol over a vertically stretching sheet. Jawad *et al.* [30] looked at how the flow of a hybrid nanofluid and melting heat transfer interact over a surface that stretches. They took into account the effects of second-order slip, Eckert number, and Prandtl number. Rehman *et al.* [31] have studied the time dependent MHD flow of Casson hybrid nanofluid with thermal radiation along an extending surface.

Through this study, we have examined the impact of heat and mass transfers on a vertical solid permeable cone using a water-based hybrid nanofluid consisting of both $SWCNT$ and Al_2O_3 nanoparticles. This type of hybrid nanoparticles has various industrial applications, such as oxygen storage and production, as described by Hu *et al.* [32]. There are many applications of fluid flow due to a solid cone in different industrial and engineering sciences, such as the solder tip, the conical heater, and the continuous variable transmission (CVT) in a modern car (Mohamed *et al.* [33]). Recently, in some studies, Mohamed *et al.* [33], Mishra *et al.* [34] and Meena *et al.* [35], etc, have investigated the nanofluid and hybrid nanofluid flow caused by a solid cone and given different importance to the outcomes and characteristics of the cone.

Also, the thermal radiation and chemical reaction effects on fluid flow problems have played an important role in different physical fields. Over the past several decades, many researchers have given attention to these two flow factors because of their multifarious applications in different industrial issues, engineering, and medical sciences. In the early stage, the impact of thermal radiation on air and CO_2 of laminar flow through the vertical plate was studied by England and Emery [36]. Cortell [37] investigated the effects of radiation and viscous dissipation on the thermal boundary layer over a nonlinearly stretching sheet. Khan *et al.* [38] analyze the properties of a shear-thinning Williamson nanofluid with thermal radiation, focusing on the characteristics of magnetic dipole. Kumar *et al.* [39] developed a model to simulate the flow and heat transfer of a nanofluid across an infinite vertical plate subject to a magnetic field and viscous dissipation. In subsequent investigations, Ali *et al.* [40] considered how thermal radiation made an impact on the MHD hybrid nanofluid flow along the stretching cylinder. In their study, Khan *et al.* [41] examines how the presence of suspended nanoparticles in Sutterby nanofluid affects its flow behavior, particularly in the context of stratification. In a situation where the bottom plate was permeable and stretchy, Lv *et al.* [42] have investigated the impact of thermal radiation, Hall current, and an uneven heat source/sink on the flow of nanofluid between two horizontal flat plates. Recently, Khan *et al.* [43] studies the effects of a magnetized radiative flow on Sutterby nanofluid that is exposed to convective heating at a wedge surface. Abdelhafez *et al.* [44] have investigated the effect of chemical reactions and yield stress on a magnetic two-phase nanofluid flow. Rao and Deka [45] have considered the effect of viscous dissipation, thermal radiation and chemical reactions on unsteady MHD Casson nanofluid flow caused by a stretching sheet. The impact of nanoparticles and radiation on viscoelastic fluids is explored by Khan *et al.* [46], who emphasize the crucial importance of comprehending these effects for a range of applications. Rao and Deka [47] have just recently done a numerical study of how heat and mass move through a nanofluid when it is hit by solar radiation.

The literature review presented above has motivated us to conduct a thorough analysis of the heat and mass transfer characteristics of MHD hybrid nanofluid flow through a vertical solid cone embedded in a porous medium, taking into account various factors such as a magnetic field, thermal radiation, chemical reaction, heat generation, viscous dissipation, and Joule heating. To investigate the thermal properties of the fluid, we initially suspended the $SWCNT$ nanoparticles of volume fraction ($\phi_1 = 0.1$) on the base fluid to form the $SWCNT/water$ nanofluid. Again, to enhance the properties of the fluid, $Al_2\ O_3$ nanoparticles of volume fraction ($\phi_2 = 0.1$) are added to the $SWCNT/water$ nanofluid to form $SWCNT - Al_2O_3/water$ hybrid nanofluid. This hybrid nanofluid has better thermal conductivity than either of its constituents, making it an ideal candidate for heat transfer applications. By using a similarity transformation, we transformed the governing partial differential equations into ordinary differential equations, which were then solved numerically using an implicit finite difference method known as the Keller-box method. This method is particularly well-suited for solving problems involving fluid flow and heat transfer, and has been used extensively in previous studies. Additionally, we calculated the physical quantities that measure the drag force, heat transfer rate, and mass accumulation rate at the surface of the solid cone. These quantities provide valuable insights into the behavior of the fluid and can be used to optimize the design of industrial processes that use these fluids. The study also includes a comparison of the behavior of the hybrid nanofluid with that of $Al_2O_3 - water$ nanofluid to better understand the effects of adding $SWCNT$ nanoparticles. Overall, this study provides valuable insights into the behavior of hybrid nanofluids in porous media, which can have important practical applications in fields such as energy and materials science.

2. Mathematical formulation

We have constructed a mathematical model of this study by considering a permeable cone of radius $r(x)$ which is immersed in a steady, incompressible and two-dimensional hybrid nanofluid. The flow diagram and its coordinate system are shown in Figure 1, where, the x- axis is measured along the surface of the cone and the y- axis is taken in the normal direction of the conical surface such that vertex of the cone is taken as the origin of the system. In this study, we have considered the influence of both heat and mass transfers such that T_w & C_w prescribe the constant wall temperature and concentration respectively and T_∞ & C_∞ are the temperature and concentration at free stream region. A regular magnetic field of strength B_o is applied in the normal direction of the conical surface. Here, we have considered the hybrid nanofluid which is formed by adding $SWCNT$ nanoparticles into the Al_2O_3 nanofluid and hence $SWCNT - Al_2O_3/water$ hybrid nanofluid is found. The thermo-physical properties of base fluid and solid particles are discussed in Table 1.

The following equations describe the MHD hybrid nanofluid flow with heat and mass transfer under the aforementioned assumptions and under the standard boundary conditions [33–34]:

$$\frac{\partial(ru)}{\partial x} + \frac{\partial(rv)}{\partial y} = 0, \tag{1}$$

$$u\frac{\partial u}{\partial x} + v\frac{\partial u}{\partial y} = \frac{\mu_{hnf}}{\rho_{hnf}}\frac{\partial^2 u}{\partial y^2} + g\left[\beta_t(T - T_\infty) - \beta_c(C - C_\infty)\right]cos\Omega - \frac{\sigma_{hnf}}{\rho_{hnf}}B_o^2 u - \frac{\mu_{hnf}}{\rho_{hnf}}\frac{u}{k_o}, \tag{2}$$

$$u\frac{\partial T}{\partial x} + v\frac{\partial T}{\partial y} = \frac{\kappa_{hnf}}{(\rho C_p)_{hnf}}\frac{\partial^2 T}{\partial y^2} + \frac{\mu_{hnf}}{(\rho C_p)_{hnf}}\left(\frac{\partial u}{\partial y}\right)^2 + \frac{\sigma_{hnf}}{(\rho C_p)_{hnf}}\mathrm{B}_o^2 u^2 + \frac{Q_o}{(\rho C_p)_{hnf}}(T - T_\infty)$$
$$- \frac{1}{(\rho C_p)_{hnf}}\frac{\partial q_r}{\partial y}, \tag{3}$$

$$u\frac{\partial C}{\partial x} + v\frac{\partial C}{\partial y} = D_m\frac{\partial^2 C}{\partial y^2} - Kr(C - C_\infty). \tag{4}$$

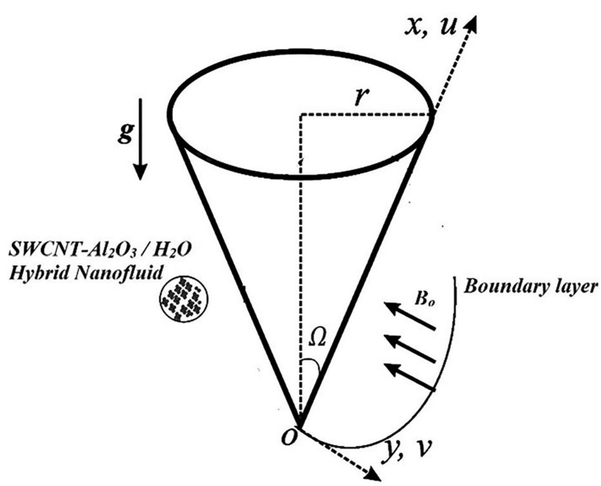

Figure 1. Schematic diagram of the problem.

Table 1. Thermophysical properties of water and nanoparticles [21].

	$\rho(kg/m^3)$	$\kappa(W/mK)$	$\sigma(s/m)$	$C_p(J/kgK)$
H_20	997.1	0.613	5.5×10^{-6}	4179
$SWCNT$	2600	6600	1×10^6	425
Al_2O_3	3970	40	35×10^6	765

The following are the initial and boundary conditions:

$$\begin{array}{llllll} u = u_w, & v = v_w, & T = T_w, & C = C_w & when \; y = 0, & \\ u \to 0, & & T \to 0, & C \to 0 & as \quad y \to \infty. \end{array} \tag{5}$$

The Rosseland approximation for radiative heat flux can be mathematically written as [48–50]

$$\frac{\partial q_r}{\partial y} = \frac{-4\sigma^*}{3k^*}\frac{\partial T^4}{\partial y} \tag{6}$$

By generalizing the Taylor series and ignoring the higher order terms, we are able to get:

$$T^4 = 4\ T_\infty^3\ T - 3\,T_\infty^4$$

Hence Eq. (5) becomes-

$$\frac{\partial q_r}{\partial y} = \frac{-16\sigma^*}{3k^*}\ T_\infty^3 \frac{\partial^2\ T}{\partial y^2} \tag{7}$$

We use the similarity transformation [34]-

$$\begin{aligned} &\eta = \sqrt{\frac{a}{\nu_f}}y, \quad \psi = \sqrt{a\nu_f}xrf(\eta), \ \ r = xsin\Omega, \\ &\theta(\eta) = \frac{T - T_\infty}{T_w - T_\infty}, \ \ \phi(\eta) = \frac{C - C_\infty}{C_w - C_\infty}, \ \ u = \frac{1}{r}\frac{\partial \psi}{\partial y} = axf'(\eta), \ \ v = -\frac{1}{r}\frac{\partial \psi}{\partial x} = -\sqrt{a\nu_f}f(\eta) \end{aligned} \tag{8}$$

Substituting (8) in the governing Eqs. (1) to (4) we get:

$$f''' + \frac{A_2}{A_1}ff'' - \frac{A_2}{A_1}f'^2 + \frac{A_2}{A_1}(Gr\theta - Gc\phi) - \frac{A_5}{A_1}Mf' - K_pf' = 0, \tag{9}$$

$$\frac{\theta''}{Pr}(A_4 + Rd) + A_3f\theta' + A_1E_cf''^2 + A_5ME_cf'^2 + Q\theta = 0, \tag{10}$$

$$\phi'' + Scf\phi' - Sc\gamma\phi = 0, \tag{11}$$

The boundary condition (5) is transformed to:

$$\begin{array}{llll} f(0) = S, & f'(0) = 1, & \theta(0) = 1, & \phi(0) = 1, \\ & f'(\infty) \to 0, & \theta(\infty) \to 0, & \phi(\infty) \to 0. \end{array} \tag{12}$$

Here $A_i (i = 1, 2, 3, 4, 5)$ are defined in the following ways:

$$A_1 = \frac{\mu_{hnf}}{\mu_f}, \ A_2 = \frac{\rho_{hnf}}{\rho_f}, \ A_3 = \frac{(\rho C_p)_{hnf}}{(\rho C_p)_f}, \ A_4 = \frac{\kappa_{hnf}}{\kappa_f}, \ A_5 = \frac{\sigma_{hnf}}{\sigma_f}.$$

In this study, we specify the flow parameters as follows –

$$M = \frac{\sigma_f B_o^2}{a\rho_f}, \ K_p = \frac{\nu_f}{ak_o}, \ Gr = \frac{g\beta_t(T_w - T_\infty)}{a^2x}, \ Gc = \frac{g\beta_c(C_w - C_\infty)}{a^2x}, \ Pr = \frac{\nu_f(\rho C_p)_f}{\kappa_f},$$

$$Rd = \frac{16\sigma^* T_\infty^3}{3k^*\kappa_f}, \ Ec = \frac{(ax)^2\rho_f}{(\rho C_p)_f(T_w - T_\infty)}, \ Q = \frac{Q_o}{a(\rho C_p)_f}, \ Sc = \frac{\nu_f}{D_m}, \ \gamma = \frac{Kr}{a}.$$

The following physical quantities are observed in this study that are very important in several engineering applications and industrial processes. The skin-friction coefficient (C_f) and the Nusselt number (Nu_x) are defined as follows-

$$Cf_x = 2\frac{\mu_{hnf}}{\rho_f u_w^2}\left(\frac{\partial u}{\partial y}\right)_{y=0}, \ Nu_x = -\frac{x\kappa_{hnf}}{\kappa_f(T_w - T_\infty)}\left(\frac{\partial T}{\partial y}\right)_{y=0}, \ Sh_x = -\frac{x}{(C_w - C_\infty)}\left(\frac{\partial C}{\partial y}\right)_{y=0} \tag{13}$$

Now, using the Eq. (8) into the Eq. (13), we have achieved the following normalize form of the above quantities as:

$$Re_x^{\frac{1}{2}}Cf_x = \frac{1}{(1-\phi_1)^{2.5}(1-\phi_2)^{2.5}}f''(0),$$

$$Re_x^{-\frac{1}{2}}Nu_x = -\frac{\kappa_{hnf}}{\kappa_f}\theta'(0),$$

$$Re_x^{-\frac{1}{2}}Sh_x = -\phi'(0),$$

where, the local Reynolds number, $Re_x = \frac{xu_w}{\nu_f}$

3. Method of solutions

The Keller-box technique is used for numerical solution of Eqs. (9)–(11), together with boundary condition (12). We choose this scheme because of its flexibility and it is found to be very effective in solving the non-linear problem with an error of order 10^{-5}. Methodology considered by Cebeci and Bradshaw [51] has been implemented. Computational steps (as explained by Anwar *et al.* [52]) involved in this scheme to get a numerical solution are as follows:

a. To reduce the obtained ordinary differential equations (ODE) into the system of first-order equations.
b. To write the reduced equations in finite difference equations.
c. To linearize the equations using Newton method and writing them in vector form.
d. To solve the linear equations which provide the tridiagonal matrix.

By following these computational steps, the Keller-box technique provides a numerical solution to the original non-linear problem with great accuracy.

4. Results and discussion

In order to study the physical representation of the problem, the numerical results are reported in both graphical as well as in tabular form. The influence of various parameters on velocity, temperature and concentration profile are plotted in graphs whereas the numerical values of skin-friction coefficient, local Nusselt number, and local Sherwood number are presented in tables. Here, all the graphs and the numerical values are obtained by implementing the Keller-box method using MATLAB code. To validate the accuracy and precision of our numerical method, we compared our results of $(-\theta'(0))$ for a specific Prandtl number with those reported by Butt *et al.* [53] and Mishra *et al.* [34]. Table 3 seems to be in excellent compliance. Moreover, we compared our temperature profiles with those previously reported by Grubka and Bobba [54] under the condition of $\gamma = 1$. Our comparison revealed a high degree of agreement as shown in Figure 2. The temperature profiles consistently decreased as the Prandtl number increased, leading to a corresponding decrease in the thermal boundary layer thickness. This trend can be observed by examining the temperature curves corresponding to different values of the Prandtl number in Figure 2. Therefore, we are confident that the accuracy of computation results is adequate to represent the solution or physical process.

The changes in velocity of both hybrid nanofluid ($SWCNT - Al_2O_3/water$) and nanofluid ($Al_2O_3/water$) for various values of magnetic parameter (M) are shown in Figure 3. It is found here that for both the cases, the velocity decreases as the value of magnetic parameter rises. It can also be observed that $Al_2O_3/water$ nanofluid flow slightly slower than the $SWCNT - Al_2O_3/water$ hybrid nanofluid flow. In response to an increase in the strength of the magnetic

Table 2. Thermophysical properties model for hybrid nanofluid [33].

Property	Hybrid nanofluid
Density	$\rho_{hnf} = (1-\phi_2)[(1-\phi_1)\rho_f + \phi_1\rho_{s1}] + \phi_2\rho_{s2}$
Dynamic viscosity	$\mu_{hnf} = \frac{\mu_f}{(1-\phi_1)^{2.5}(1-\phi_2)^{2.5}}$
Heat capacity	$(\rho C_p)_{hnf} = (1-\phi_2)\left[(1-\phi_1)(\rho C_p)_f + \phi_1(\rho C_p)_{s1}\right] + \phi_2(\rho C_p)_{s2}$
Thermal conductivity	$\kappa_{hnf} = \frac{\kappa_{s2} + 2\kappa_{nf} - 2\phi_2(\kappa_{nf} - \kappa_{s2})}{\kappa_{s2} + 2\kappa_{nf} + \phi_2(\kappa_{nf} - \kappa_{s2})} \times \kappa_{nf}$ where, $\kappa_{nf} = \frac{\kappa_{s1} + 2\kappa_f - 2\phi_1(\kappa_f - \kappa_{s1})}{\kappa_{s1} + 2\kappa_f + \phi_1(\kappa_f - \kappa_{s1})} \times \kappa_f$
Electrical conductivity	$\sigma_{hnf} = \left[1 + \frac{3\left(\frac{\sigma_{s2}}{\sigma_{nf}} - 1\right)\phi_2}{\left(\frac{\sigma_{s2}}{\sigma_{nf}} + 2\right) - \left(\frac{\sigma_{s2}}{\sigma_{nf}} - 1\right)\phi_2}\right] \times \sigma_{nf}$ where, $\sigma_{nf} = \left[1 + \frac{3\left(\frac{\sigma_{s1}}{\sigma_f} - 1\right)\phi_1}{\left(\frac{\sigma_{s1}}{\sigma_f} + 2\right) - \left(\frac{\sigma_{s1}}{\sigma_f} - 1\right)\phi_1}\right] \times \sigma_f$

Table 3. Comparison of numerical values of $-\theta'(0)$ when $\phi_1 = \phi_2 = M = Kp = \gamma = Gr = Gm = Sc = Rd = S = Ec = Q = 0$.

	$-\theta\,'(0)$		
Pr	Butt *et al.* [53]	Mishra *et al.* [34]	Present
1.0	0.5820	0.5818299	0.5809
10.0	2.3080	2.3079730	0.3065

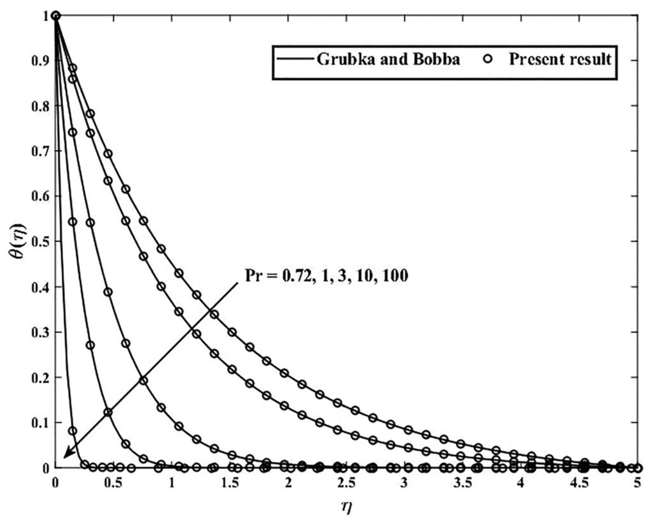

Figure 2. Comparison of the temperature profiles given in Grubka and Bobba [54] with the present results.

field, a retarding effect of the Lorentz force is generated (pressure drop phenomenon), which effect the flow to slow down. Because of this, when M increases, velocity profile falls. It is found in Figure 4 that as M is raised, so too is the range of temperatures experienced inside the boundary layer. Increase in the effect of Lorentz force results to a frictional resistance to the flow, which leads to the increase in temperature in the boundary layer region. Accordingly, increasing M causes an increase in temperature. It was clear from the figure that the $SWCNT - Al_2O_3/water$ hybrid nanofluid holds temperature better than the $Al_2O_3/water$ nanofluid.

Figures 5 and 6 reveal the impact of porosity parameter (K_p) on the velocity and temperature profile respectively. It is clear from the figures that the velocity for both $SWCNT - Al_2O_3/water$ hybrid nanofluid and $Al_2O_3/water$ nanofluid decrease with the increase in the value of K_p whereas an opposite behavior is observed for temperature profile of both cases. This occurs because an enhancement in K_p amplifies the porous layer and thus, velocity in the boundary layer

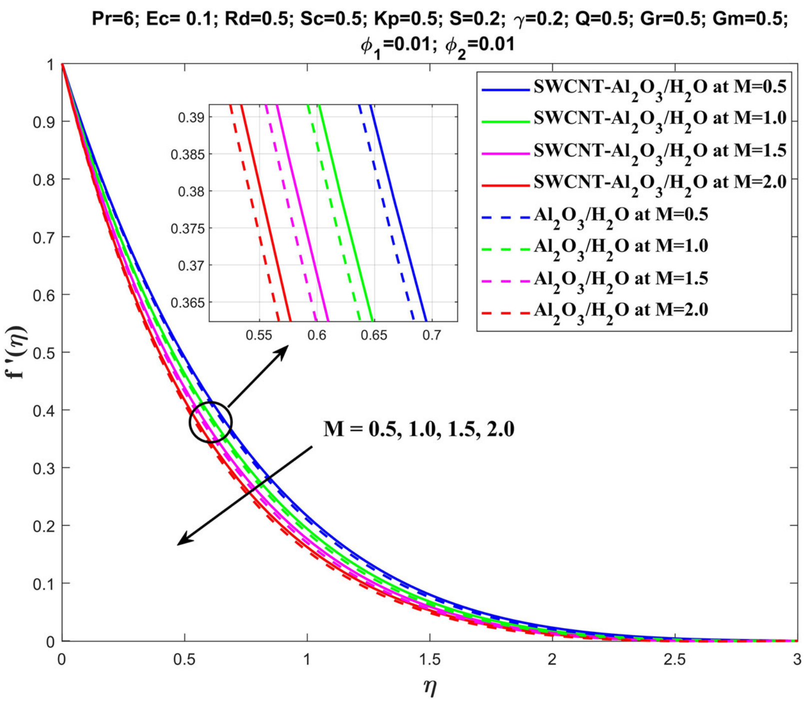

Figure 3. Velocity profile for various value of M.

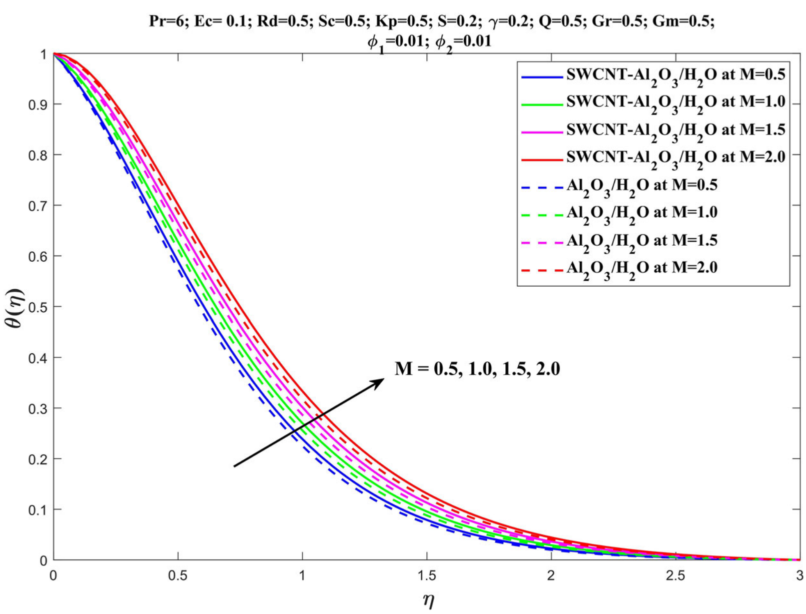

Figure 4. Temperature profile for various value of M.

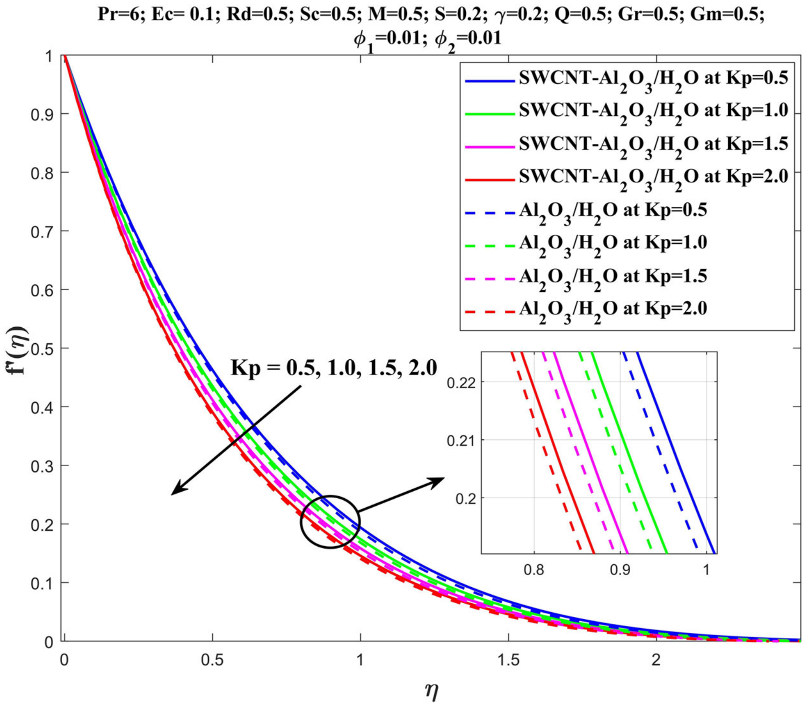

Figure 5. Velocity profile for various value of ***Kp***.

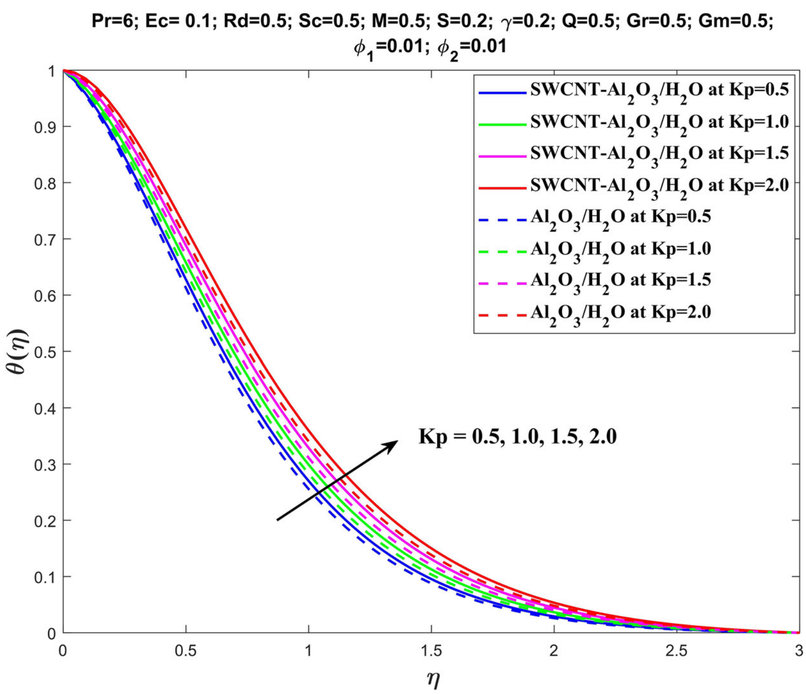

Figure 6. Temperature profile for various value of ***Kp***.

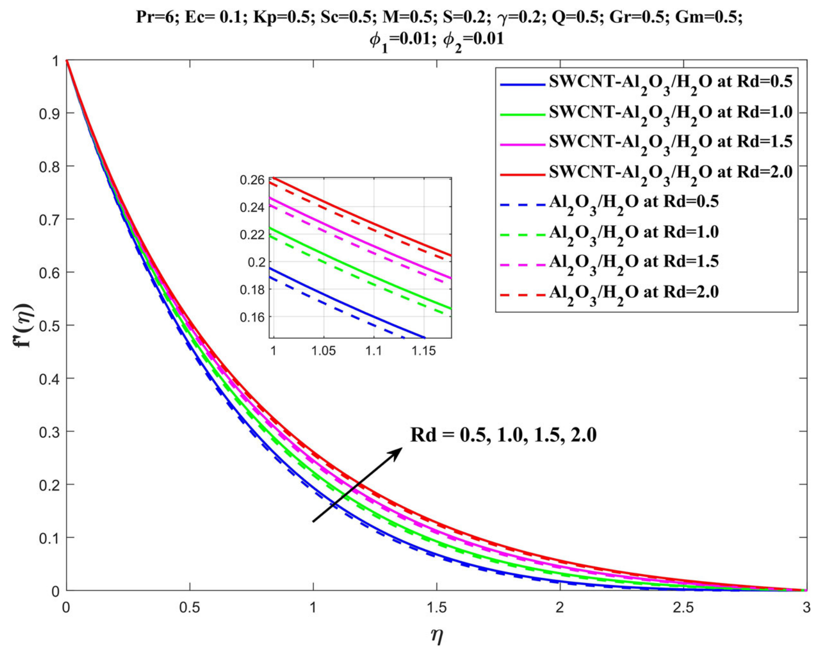

Figure 7. Velocity profile for various value of ***Rd***.

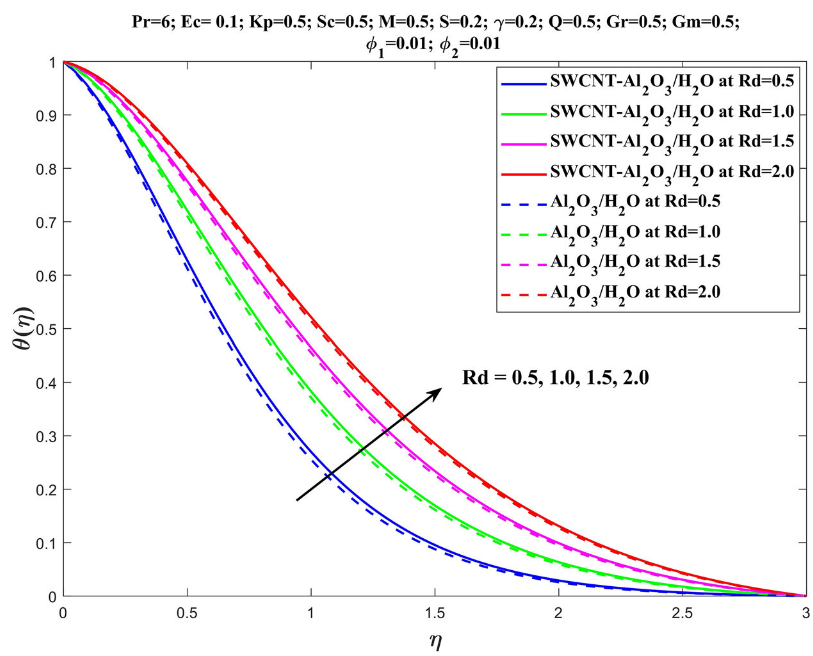

Figure 8. Temperature profile for various value of ***Rd***.

decreases whereas the temperature increases. From the figures it can be concluded that the hybrid nanofluid shows better results in controlling the velocity as well as holding the temperature for this instance too.

Figure 7 depicts the velocity profile for the variation of values of radiation parameter (Rd). It can be observed from the figure that the velocity inside the boundary layer region increases with

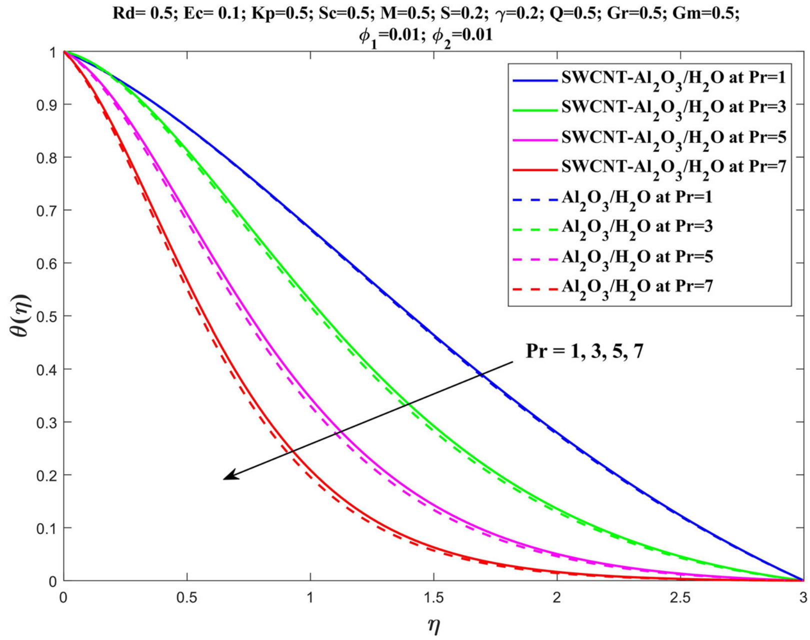

Figure 9. Temperature profile for various value of ***Pr***.

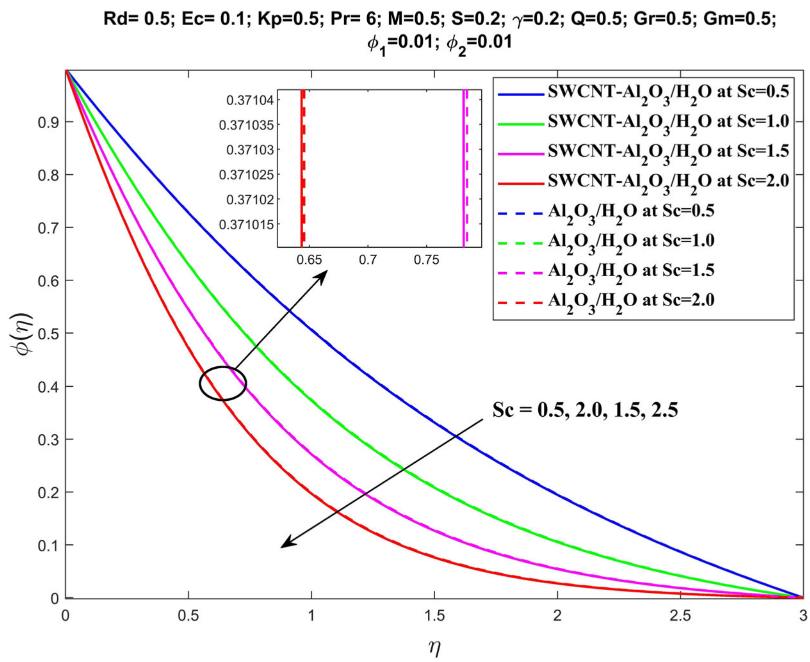

Figure 10. Concentration profile for various value of ***Sc***.

the increase in radiation parameter for both the cases. The main reason behind the fact is that with the increase in thermal radiation the kinetic energy of the flow also increases. Hence the velocity of the flow increases with the increase in Rd. The impact of radiation parameter (Rd) on the temperature profile is shown in Figure 8. The figure shows the impact for both $SWCNT - Al_2O_3/water$ hybrid nanofluid and $Al_2O_3/water$ nanofluid and it is evident that when the

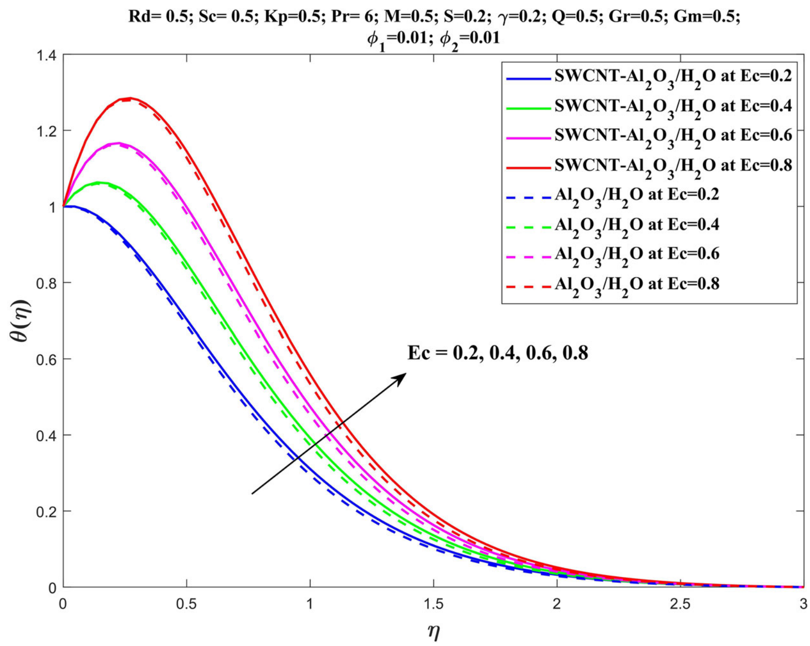

Figure 11. Temperature profile for various value of ***Ec***.

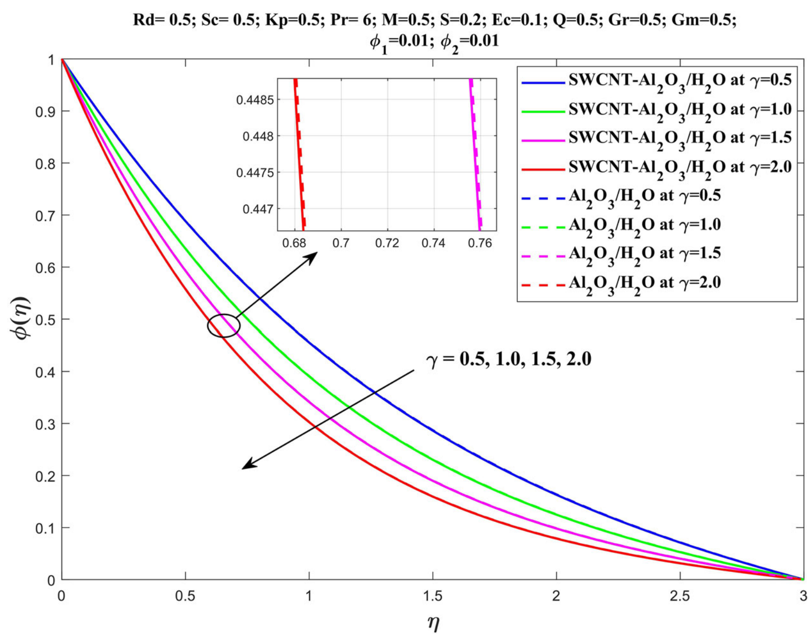

Figure 12. Concentration profile for various value of γ.

radiation parameter increases, the temperature rises. That's because what we are observing is the result of heat energy being released into the fluid as a result of an increase in thermal radiation. It is noteworthy to see that the hybrid nanofluid shows higher temperature profile than the ordinary nanofluid.

Figure 9 exhibits the effect of Prandtl number (Pr) on dimensionless temperature for both $SWCNT - Al_2O_3/water$ hybrid nanofluid and $Al_2O_3/water$ nanofluid. As Pr rises, it's easy to see how

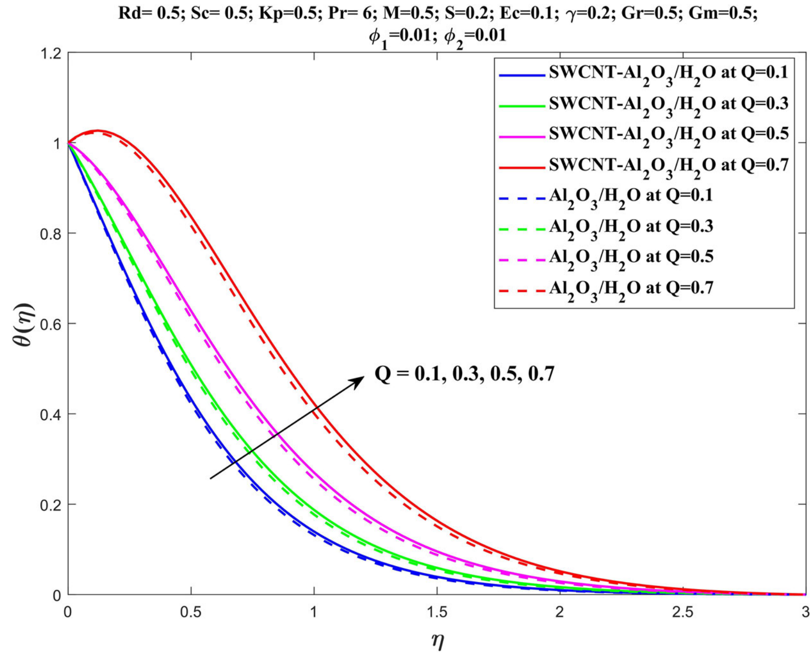

Figure 13. Temperature profile for various value of Q.

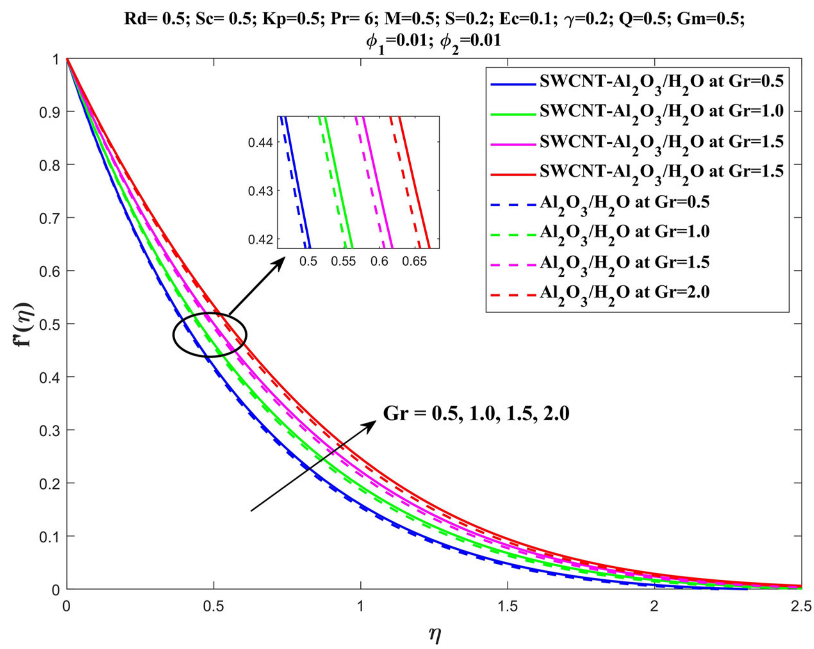

Figure 14. Velocity profile for various value of Gr.

the temperature within the boundary layer area drops. *Pr* is defined as momentum-to-temperature diffusivity ratio. So, a high value of *Pr* indicates a poor thermal conductivity and a smaller thermal layer structure, since momentum diffuses more quickly than heat. As the *Pr* rises, the heat transfer rate of the fluid rises, causing the temperature of the boundary layer to fall. The fluctuations on concentration profile are seen for different values of Schmidt number (*Sc*) in Figure 10. From the figure it is clear

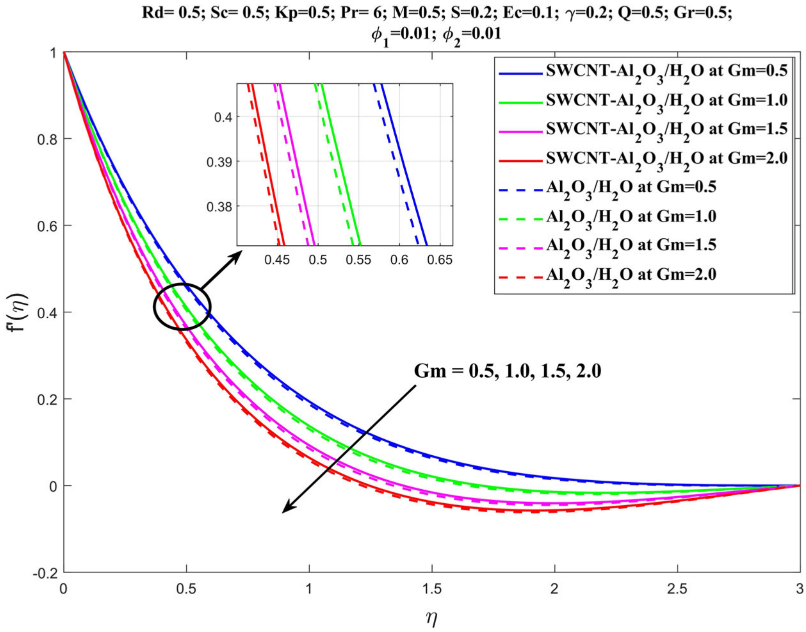

Figure 15. Velocity profile for various value of Gm.

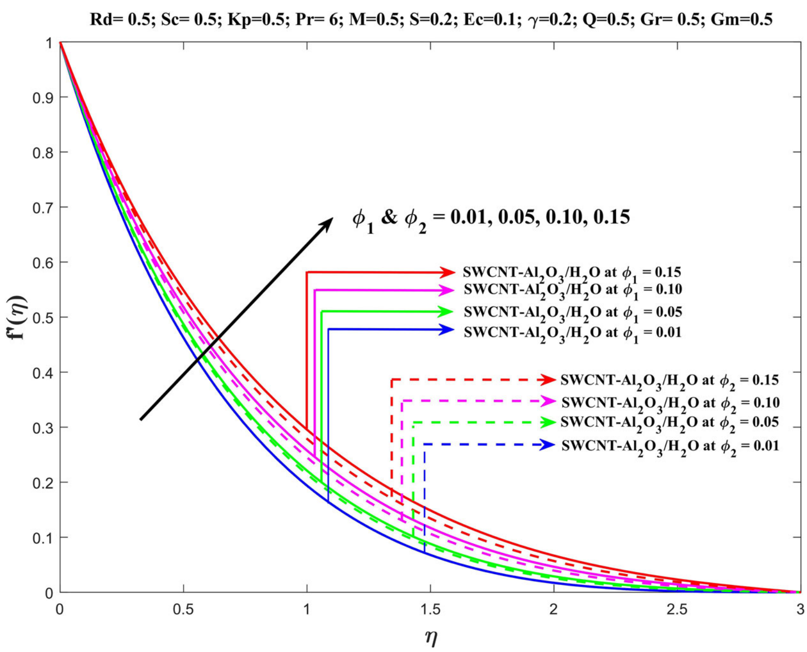

Figure 16. Velocity profile for various value of ϕ_1 and. ϕ_2

that for both the cases temperature decrease with the increase in *Sc*. It is to be noted that the hybrid nanofluid and ordinary nanofluid both show similar performance in concentration profile with the increase in *Sc*.

The influence of Eckert number (Ec) on temperature profile is depicted in Figure 11. The dimensionless temperature rises as Ec rises, as can be seen in both $SWCNT - Al_2O_3/water$ hybrid nanofluid as well as $Al_2O_3/water$ nanofluid. This is because the viscosity of nanofluid stores

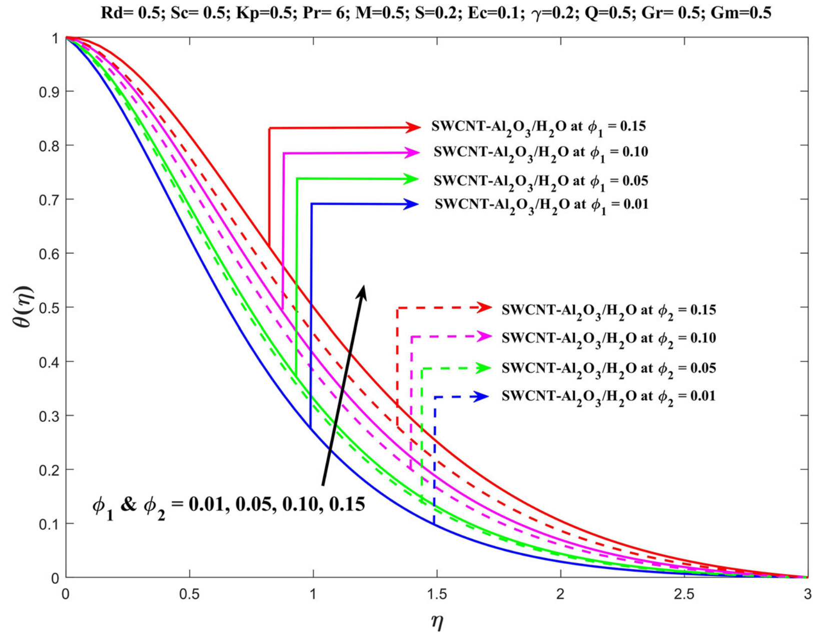

Figure 17. Temperature profile for various value of ϕ_1 and. ϕ_2

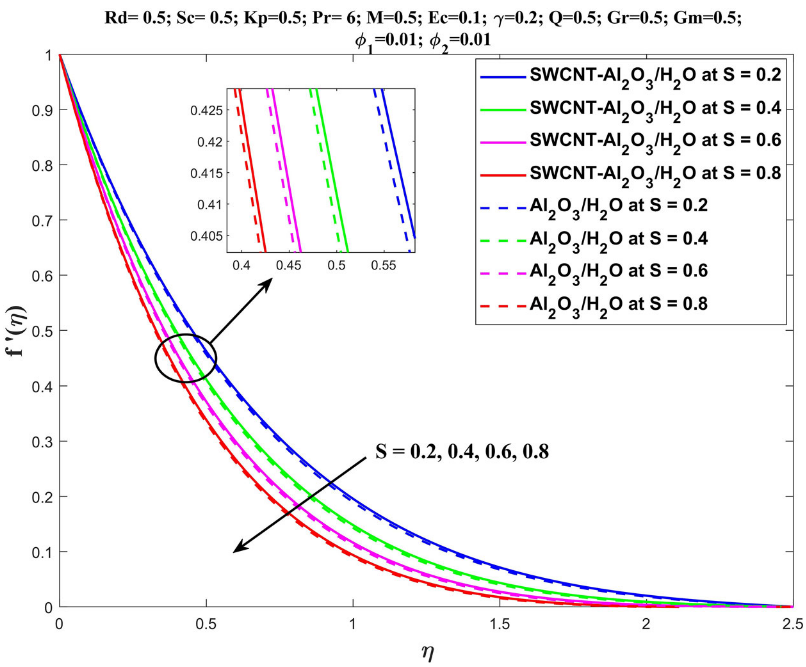

Figure 18. Velocity profile for various value of ***S***.

energy from the flow owing to frictional heating and changes it into internal energy. This phenomenon contributes to the increase in thermal boundary layer thickness. Figure 12 illustrates how the chemical reaction parameter (γ) influences the concentration of nanoparticles for both $SWCNT - Al_2O_3/water$ hybrid nanofluid and $Al_2O_3/water$ nanofluid. This graph clearly shows

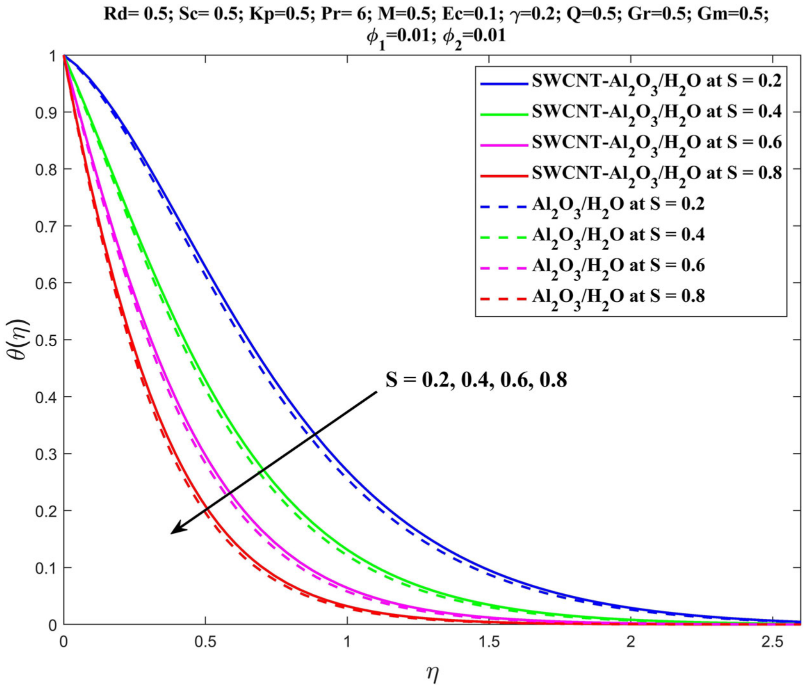

Figure 19. Temperature profile for various value of ***S***.

how increase in the value of the reaction parameter reduces the nanoparticles presence at the surface. The fundamental cause is that when a chemical reaction parameter's value rises, so do the number of solute molecules engaged in the reaction. As a result, the concentration profile declines. Thus, using several chemical processes results in a considerable depletion of the solutal boundary layer, which increases mass transport phenomena. Figure 13 describes the performance of both hybrid nanofluid ($SWCNT - Al_2O_3$) as well as the ordinary nanofluid (Al_2O_3) on temperature profile for different values of heat generation/absorption (Q). It is clear from the figure that the temperature increases with the increase in the value of Q.

Figures 14 and 15 demonstrate the effects of the Grashof number (Gr) and modified Grashof number (Gm) on velocity profile. It can be seen that the velocity profile increases with the increase in Gr but an opposite trend can be observed for the case of Gm.

Figure 16 shows the influence of ϕ_1 and ϕ_2 on velocity profile. It can be found the increase in the value of ϕ_1 and ϕ_2 results in the increase in velocity profile of the hybrid nanofluid. Figure 17 reflect the influence of temperature profile for the increasing value of both ϕ_1 and ϕ_2. It is clear from the figure that the temperature intensifies with the increases in the volume fraction of both nanoparticle of the hybrid nanofluid. The main reason behind this phenomenon is that increasing volume fraction increases the thermal boundary layer thickness, which results the rate of heat transfer to slow down inside the boundary layer region. Hence the temperature raises.

The higher wall suction parameter (S) reduces the velocity distribution for both $SWCNT - Al_2O_3/water$ hybrid nanofluid as well as $Al_2O_3/water$ nanofluid as displayed in Figure 18. Physically, the adhesion of the nanofluid to the wall of geometry caused by the intense wall suction results in a significant decrease in flow. For this reason, increased wall suction causes a decrease in the overall velocity distribution. The temperature curve for varying suction parameter (S) is shown graphically in Figure 19. It is obvious from the graph that the temperature of both $SWCNT - Al_2O_3/water$ hybrid nanofluid as well as $Al_2O_3/water$ nanofluid decreases as we increase the value of suction parameter. This is due to the fact that increasing suction value leads to the increase in the distance from the surface which leads the temperature to decrease and

Table 4. Values of $Re_x^{\frac{1}{2}}Cf_x$, $-Re_x^{-\frac{1}{2}}Nu_x$ and $-Re_x^{-\frac{1}{2}}Sh_x$ for the $SWCNT - Al_2O_3/water$ hybrid nanofluid, when $M = Kp = 0.5$, $\gamma = Q = S = 0.2$, $Gr = 1$, $Gm = 2$, $\phi_1 = \phi_2 = 0.01$.

Pr	Sc	Ec	Rd	$Re_x^{\frac{1}{2}}Cf_x$	$-Re_x^{-\frac{1}{2}}Nu_x$	$-Re_x^{-\frac{1}{2}}Sh_x$
0.015	0.5	0.01	0.5	−1.9576	0.3339	0.5706
7.0				−2.2292	1.0573	0.5399
13.5				−2.3561	1.9502	0.5286
5.0	0.22	0.01	0.5	−2.2133	0.6580	0.4235
	0.30			−2.1998	0.6977	0.4577
	0.60			−2.1428	0.8303	0.5928
5.0	0.5	0.01	0.5	−2.1628	0.7891	0.5467
		0.05		−2.1449	0.6030	0.5481
		0.1		−2.1240	0.3794	0.5498
5.0	0.5	0.01	0.5	−2.1628	0.7891	0.5467
			1.0	−2.1166	0.6427	0.5517
			1.5	−2.0862	0.5612	0.5550

finally vanishes in a large distance from the surface, which implies increasing in the wall temperature gradient and in turn increases the surface heat transfer rate.

Table 4 is inserted to show the numerical values of physical quantities of interest which are observed during this investigation are skin friction coefficient ($Re_x^{1/2}Cf_x$), Nusselt number ($-Re_x^{-1/2}Nu_x$) and Sherwood number ($-Re_x^{-1/2}Sh_x$). These quantities help to evaluate the effects of shear stress, heat transfer rate and mass accumulation rate etc. From Table 4, it is found that the Nusselt number experience an enhancement from the noble gas ($Pr = 0.015$) to sea-water ($Pr = 13.5$) whereas the skin friction coefficient and effects of mass accumulation rate (Sherwood number) reduce with Pr. Again, the effects of shear stress, heat transfer rate and mass accumulation rate at the surface enhances from the hydrogen ($Sc = 0.22$) to water vapor ($Sc = 0.60$). It is also seen from this table is that increasing values of the Eckert number and radiation parameter raise the influence of shear stress and the mass accumulation rate and reduces the heat transfer rate of the hybrid nanofluid at the surface of the cone.

5. Conclusion

In this study, we investigated the heat and mass transfer characteristics of a steady, two-dimensional MHD hybrid nanofluid flow over a vertical porous cone, taking into account various influential factors such as thermal radiation, chemical reactions, heat generation, viscous dissipation, and Joule heating. The base fluid used was water, and the nanoparticles used were $SWCNT$ and Al_2O_3. The numerical analysis was performed using the Keller-box Scheme due to its flexibility compared to other numerical schemes.

Our findings provide insight into the behavior of the hybrid nanofluid flow and its comparison with the nanofluid with single nanoparticles. It was observed that increasing the effect of magnetic field, porosity, suction, and modified Grashof number can control the velocity of the hybrid nanofluid flow inside the boundary layer region. Furthermore, the velocity of the flow was found to increase with the increase in the value of radiation parameter, Grashof number, and volume fraction of the nanoparticles. The temperature of the boundary layer region was found to increase with the effect of magnetic field, porosity, thermal radiation, viscosity, heat generation, and volume fraction of the nanoparticles used. On the other hand, the temperature of the hybrid nanofluid was observed to decrease with the increment in the value of Prandtl number and suction parameter. The nanoparticle concentration in the boundary layer region is found to decrease with the increase in the value of Schmidt number and chemical reaction parameter.

In addition, the skin friction coefficient was found to decrease slowly with the increase in Prandtl number, while it increased with the increase in Schmidt number, Eckert number, and radiation parameter. The rate of heat transfer was observed to increase with the increase in

Prandtl number and Schmidt number, but it decreased with the increase in radiation parameter and Eckert number. The mass transfer rate was found to increase with the increase in Schmidt number, Eckert number, and radiation parameter, but it decreased with the increase in Prandtl number.

Our results also indicate that the hybrid nanofluid flow is slightly faster than that of the nanofluid with single nanoparticles. The boundary layer region of the hybrid nanofluid is found to be warmer than the nanofluid with single nanoparticles. However, both hybrid nanofluid as well as ordinary nanofluid display almost similar performance when it comes to the species concentration profile of the flow.

Overall, our findings suggest that the use of hybrid nanofluid gives better results than that of the nanofluid with single nanoparticles, making it a promising candidate for various industrial applications.

Future directions of this research could be to investigate the impact of different geometries of solid cones and porous media. The exploration of new hybrid nanofluid combinations could also be conducted to optimize the thermal conductivity of the nanofluid. Besides, the study could be extended to three-dimensional flows to understand the flow behavior and heat transfer characteristics more comprehensively.

ORCID

Shiva Rao http://orcid.org/0000-0003-2055-4441
P. N. Deka http://orcid.org/0000-0001-9485-9294

References

[1] S. U. S. Choi and J. Eastman, “Enhancing thermal conductivity of fluids with nanoparticles,” *Argonne National Lab (United States)*, vol. 66, pp. 99–105, 1995.
[2] S. Lee, S. U.-S. Choi, S. Li and J. A. Eastman, “Measuring thermal conductivity of fluids containing oxide nanoparticles,” *J. Heat Transfer*, vol. 121, no. 2, pp. 280–289, 1999. DOI: 10.1115/1.2825978.
[3] J. Buongiorno, “Convective transport in nanofluids,” *J. Heat Transfer*, vol. 128, no. 3, pp. 240–250, 2006. DOI: 10.1115/1.2150834.
[4] A. V. Kuznetsov and D. A. Nield, “Natural convective boundary-layer flow of a nanofluid past a vertical plate,” *Int. J. Therm. Sci.*, vol. 49, no. 2, pp. 243–247, 2010. DOI: 10.1016/j.ijthermalsci.2009.07.015.
[5] W. A. Khan and I. Pop, “Boundary-layer flow of a nanofluid past a stretching sheet,” *Int. J. Heat Mass Transfer*, vol. 53, no. 11–12, pp. 2477–2483, 2010. DOI: 10.1016/j.ijheatmasstransfer.2010.01.032.
[6] O. D. Makinde and A. Aziz, “Boundary layer flow of a nanofluid past a stretching sheet with a convective boundary condition,” *Int. J. Therm. Scie.*, vol. 50, no. 7, pp. 1326–1332, 2011. DOI: 10.1016/j.ijthermalsci.2011.02.019.
[7] W. A. Khan, M. Ali, M. Irfan, M. Khan, M. Shahzad and F. Sultan, “A rheological analysis of nanofluid subjected to melting heat transport characteristics,” *Appl. Nanosci.*, vol. 10, no. 8, pp. 3161–3170, 2020. DOI: 10.1007/s13204-019-01067-5.
[8] Z. Hussain and W. Azeem Khan, “Impact of thermal-solutal stratifications and activation energy aspects on time-dependent polymer nanoliquid,” in *Waves in Random and Complex Media*. London, UK: Taylor & Francis, 2022, pp. 1–11. DOI: 10.1080/17455030.2022.2128229.
[9] M. Tabrez and W. Azeem Khan, “Exploring physical aspects of viscous dissipation and magnetic dipole for ferromagnetic polymer nanofluid flow,” in *Waves Random Complex Media*. London, UK: Taylor & Francis, 2022, pp. 1–20. DOI: 10.1080/17455030.2022.2135794.
[10] S. Rao and P. N. Deka, “A numerical study on heat transfer for mhd flow of radiative casson nanofluid over a porous stretching sheet,” *LAAR*, vol. 53, no. 2, pp. 129–136, 2023. DOI: 10.52292/j.laar.2023.950.
[11] N. Anjum, W. A. Khan, A. Hobiny, M. Azam, M. Waqas and M. Irfan, “Numerical analysis for thermal performance of modified Eyring Powell nanofluid flow subject to activation energy and bioconvection dynamic,” *Case Stud. Therm. Eng.*, vol. 39, pp. 102427, 2022. DOI: 10.1016/j.csite.2022.102427.
[12] S. Rao and P. Deka, “A numerical study on unsteady MHD Williamson nanofluid flow past a permeable moving cylinder in the presence of thermal radiation and chemical reaction,” *Biointerface Res. Appl. Chem.*, vol. 13, no. 5, pp. 436, 2023. DOI: 10.33263/BRIAC135.436.

[13] M. Waqas, W. A. Khan, A. A. Pasha, N. Islam and M. M. Rahman, "Dynamics of bioconvective Casson nanoliquid from a moving surface capturing gyrotactic microorganisms, magnetohydrodynamics and stratifications," *Therm. Sci. Eng. Prog.*, vol. 36, pp. 101492, 2022. DOI: 10.1016/j.tsep.2022.101492.

[14] S. Iijima, "Helical microtubules of graphitic carbon," *Nature*, vol. 354, no. 6348, pp. 56–58, 1991. DOI: 10.1038/354056a0.

[15] V. Prajapati, P. K. Sharma and A. Banik, "Carbon nanotubes and its applications," *Int. J. Pharm. Sci. Res.*, vol. 2, no. 5, pp. 1099–1107, 2011. DOI: 10.13040/ijpsr.0975-8232.

[16] A. Khalid, I. Khan, A. Khan, S. Shafie and I. Tlili, "Case study of MHD blood flow in a porous medium with CNTS and thermal analysis," *Case Stud. Therm. Eng.*, vol. 12, pp. 374–380, 2018. DOI: 10.1016/j.csite.2018.04.004.

[17] T. Hayat, A. Kiran, M. Imtiaz and A. Alsaedi, "Unsteady flow of carbon nanotubes with chemical reaction and Cattaneo-Christov heat flux model," *Results Phys.*, vol. 7, pp. 823–831, 2017. DOI: 10.1016/j.rinp.2017.01.031.

[18] A. Alsagri, *et al.*, "MHD thin film flow and thermal analysis of blood with CNTs nanofluid," *Coatings*, vol. 9, no. 3, pp. 175, 2019. DOI: 10.3390/coatings9030175.

[19] A. Khan, *et al.*, "Darcy-Forchheimer flow of MHD CNTs nanofluid radiative thermal behaviour and convective non uniform heat source/sink in the rotating frame with microstructure and inertial characteristics," *AIP Adv.*, vol. 8, no. 12, pp. 125024, 2018. DOI: 10.1063/1.5066223.

[20] V. Kumaresan, R. Velraj and S. K. Das, "Convective heat transfer characteristics of secondary refrigerant based CNT nanofluids in a tubular heat exchanger," *Int. J. Refrig.*, vol. 35, no. 8, pp. 2287–2296, 2012. DOI: 10.1016/j.ijrefrig.2012.08.009.

[21] B. J. Mahanthesh, N. Gireesha, S. Shashikumar and S. A. Shehzad, "Marangoni convective MHD flow of SWCNT and MWCNT nanoliquids due to a disk with solar radiation and irregular heat source," *Phys. E: Low-Dimens. Syst. Nanostruct.*, vol. 94, pp. 25–30, 2017. DOI: 10.1016/j.physe.2017.07.011.

[22] R. Hossain, A. K. Azad, M. Jahid Hasan and M. M. Rahman, "Thermophysical properties of kerosene oil-based CNT nanofluid on unsteady mixed convection with MHD and radiative heat flux," *Eng. Sci. Technolo. Int. J.*, vol. 35, pp. 101095, 2022. DOI: 10.1016/j.jestch.2022.101095.

[23] A. Rehman, A. Saeed, Z. Salleh, R. Jan and P. Kumam, "Analytical investigation of the time-dependent stagnation point flow of a CNT nanofluid over a stretching surface," *Nanomaterials*, vol. 12, no. 7, pp. 1108, 2022. DOI: 10.3390/nano12071108.

[24] B. Maatki, "Heat transfer enhancement using CNT-water nanofluids and two stages of seawater supply in the triangular solar still," *Case Stud. Therm. Eng.*, vol. 30, pp. 101753, 2022. DOI: 10.1016/j.csite.2021.101753.

[25] L. S. Sundar, K. V. Sharma, M. K. Singh and A. C. M. Sousa, "Hybrid nanofluids preparation, thermal properties, heat transfer and friction factor – A review," *Renew. Sustain. Energy Rev.*, vol. 68, pp. 185–198, 2017. DOI: 10.1016/j.rser.2016.09.108.

[26] I. Waini, A. Ishak and I. Pop, "Unsteady flow and heat transfer past a stretching/shrinking sheet in a hybrid nanofluid," *Int. J. Heat Mass Transfer*, vol. 136, pp. 288–297, 2019. DOI: 10.1016/j.ijheatmasstransfer.2019.02.101.

[27] P. Sreedevi, P. Sudarsana Reddy and A. Chamkha, "Heat and mass transfer analysis of unsteady hybrid nanofluid flow over a stretching sheet with thermal radiation," *SN Appl. Sci.*, vol. 2, no. 7, pp. 1–16, 2020. DOI: 10.1007/s42452-020-3011-x.

[28] U. Yashkun, K. Zaimi, N. A. Abu Bakar, A. Ishak and I. Pop, "MHD hybrid nanofluid flow over a permeable stretching/shrinking sheet with thermal radiation effect," *HFF*, vol. 31, no. 3, pp. 1014–1031, 2021. DOI: 10.1108/HFF-02-2020-0083.

[29] H. T. Alkasasbeh, "Numerical solution of heat transfer flow of Casson hybrid nanofluid over vertical stretching sheet with magnetic field Effect," *CFDL*, vol. 14, no. 3, pp. 39–52, 2022. DOI: 10.37934/cfdl.14.3.3952.

[30] M. Jawad, Z. Khan, E. Bonyah and R. Jan, "Analysis of hybrid nanofluid stagnation point flow over a stretching surface with melting heat transfer," *Math. Prob. Eng.*, vol. 2022, pp. 1–12, 2022. vol DOI: 10.1155/2022/9469164.

[31] A. Rehman, Z. Salleh, A. A. A. Mousa, E. Bonyah and W. Khan, "Approximate analytical study of time-dependent MHD Casson hybrid nanofluid over a stretching sheet and considering thermal radiation," *Adv. Math. Phy.*, vol. 2022, pp. 1–11, 2022. vol DOI: 10.1155/2022/6271265.

[32] W. Hu, F. Donat, S. A. Scott and J. S. Dennis, "The interaction between CuO and Al2O3 and the reactivity of copper aluminates below 1000 °C and their implication on the use of the Cu–Al–O system for oxygen storage and production," *RSC Adv.*, vol. 6, no. 114, pp. 113016–113024, 2016. DOI: 10.1039/C6RA22712K.

[33] M. K. A. Mohamed, A. M. Ishak, I. Pop, N. F. Mohammad and S. K. Soid, "Free convection boundary layer flow from a vertical truncated cone in a hybrid nanofluid," *Mal. J. Fund. Appl. Sci.*, vol. 18, no. 2, pp. 257–270, 2022. DOI: 10.11113/mjfas.v18n2.2410.

[34] A. Mishra, A. K. Pandey and M. Kumar, "Velocity, thermal and concentration slip effects on MHD silver–water nanofluid flow past a permeable cone with suction/injection and viscous-Ohmic dissipation," *Heat Trans Res.*, vol. 50, no. 14, pp. 1351–1367, 2019. DOI: 10.1615/HeatTransRes.2018020420.

[35] O. P. Meena, P. Janapatla and D. Srinivasacharya, "Mixed convection fluid flow over a vertical cone saturated porous media with double dispersion and injection/suction effects," *Int. J. Appl. Comput. Math.*, vol. 7, no. 3, pp. 1–18, 2021. DOI: 10.1007/s40819-021-00990-y.

[36] W. G. England and A. F. Emery, "Thermal radiation effects on the laminar free convection boundary layer of an absorbing gas," *J. Heat Transfer*, vol. 91, no. 1, pp. 37–44, 1969. DOI: 10.1115/1.3580116.

[37] R. Cortell, "Effects of viscous dissipation and radiation on the thermal boundary layer over a nonlinearly stretching sheet," *Phys. Lett. A*, vol. 372, no. 5, pp. 631–636, 2008. DOI: 10.1016/j.physleta.2007.08.005.

[38] W. A. Khan, M. Waqas, W. Chammam, Z. Asghar, U. A. Nisar and S. Z. Abbas, "Evaluating the characteristics of magnetic dipole for shear-thinning Williamson nanofluid with thermal radiation," *Comput. Methods Prog. Biomed.*, vol. 191, pp. 105396, 2020. DOI: 10.1016/j.cmpb.2020.105396.

[39] M. A. Kumar, Y. D. Reddy, V. S. Rao and B. S. Goud, "Thermal radiation impact on MHD heat transfer natural convective nano fluid flow over an impulsively started vertical plate," *Case Stud. Therm. Eng.*, vol. 24, pp. 100826, 2021. DOI: 10.1016/j.csite.2020.100826.

[40] A. Ali, T. Kanwal, M. Awais, Z. Shah, P. Kumam and P. Thounthong, "Impact of thermal radiation and non-uniform heat flux on MHD hybrid nanofluid along a stretching cylinder," *Sci. Rep.*, vol. 11, no. 1, pp. 1–15, 2021. DOI: 10.1038/s41598-021-99800-0.

[41] W. A. Khan, N. Anjum, M. Waqas, S. Z. Abbas, M. Irfan and T. Muhammad, "Impact of stratification phenomena on a nonlinear radiative flow of sutterby nanofluid," *J. Mater. Res. Technol.*, vol. 15, pp. 306–314, 2021. DOI: 10.1016/j.jmrt.2021.08.011.

[42] Y. P. Lv, N. Shaheen, M. Ramzan, M. Mursaleen, K. S. Nisar and M. Y. Malik, "Chemical reaction and thermal radiation impact on a nanofluid flow in a rotating channel with Hall current," *Sci. Rep.*, vol. 11, no. 1, pp. 1–17, 2021. DOI: 10.1038/s41598-021-99214-y.

[43] W. A. Khan, Z. Arshad, A. Hobiny, S. Saleem, A. Al-Zubaidi and M. Irfan, "Impact of magnetized radiative flow of sutterby nanofluid subjected to convectively heated wedge," *Int. J. Mod. Phys. B*, vol. 36, no. 16, pp. 1–22, 2022. DOI: 10.1142/S0217979222500795.

[44] M. A. Abdelhafez, A. A. Awad, M. A. Nafe and D. A. Eisa, "Effects of yield stress and chemical reaction on magnetic two-phase nanofluid flow in a porous regime with thermal ray," *Indian J. Phys.*, vol. 96, no. 12, pp. 3579–3589, 2022. DOI: 10.1007/s12648-022-02288-1.

[45] S. Rao and P. Deka, "A numerical solution using EFDM for unsteady MHD radiative Casson nanofluid flow over a porous stretching sheet with stability analysis," *Heat Trans*, vol. 51, no. 8, pp. 8020–8042, 2022. DOI: 10.1002/htj.22679.

[46] W. A. Khan, *et al.*, "Impact of nanoparticles and radiation phenomenon on viscoelastic fluid," *Int. J. Mod. Phys. B*, vol. 36, no. 05, pp. 1–17, 2022. DOI: 10.1142/S0217979222500497.

[47] S. Rao and P. N. Deka, "A numerical investigation on transport phenomena in a nanofluid under the transverse magnetic field over a stretching plate associated with solar radiation," *Nonlinear Dyn. Appl.*, vol. 1, pp. 473–492, 2022. DOI: 10.1007/978-3-030-99792-2_39.

[48] Q. M. Brewster, *Thermal radiative transfer and properties, solutions manual*, 1st ed. New York: Wiley-Interscience, 1992.

[49] E. M. Sparrow and R. D. Cess, *Radiation heat transfer, augmented edition*, 1st ed. Boca Raton, FL: CRC Press Inc, 1978, DOI: 10.1201/9780203741382.

[50] A. Raptis, "Radiation and free convection flow through a porous medium," *Int. Commun. Heat Mass Transfer*, vol. 25, no. 2, pp. 289–295, 1998. DOI: 10.1016/S0735-1933(98)00016-5.

[51] T. Cebeci and P. Bradshaw, "Physical and computational aspects of convective heat transfer," in *Physical Computational Aspects Convective Heat Transfer*. New York: Springer-Verlag, 1988. DOI: 10.1007/978-1-4612-3918-5.

[52] M. I. Anwar, S. Shafie, T. Hayat, S. A. Shehzad and M. Z. Salleh, "Numerical study for MHD stagnation-point flow of a micropolar nanofluid towards a stretching sheet," *J Braz. Soc. Mech. Sci. Eng.*, vol. 39, no. 1, pp. 89–100, 2017. DOI: 10.1007/s40430-016-0610-y.

[53] A. S. Butt, A. Ali and A. Mehmood, "Numerical investigation of magnetic field effects on entropy generation in viscous flow over a stretching cylinder embedded in a porous medium," *Energy*, vol. 99, pp. 237–249, 2016. DOI: 10.1016/j.energy.2016.01.067.

[54] L. J. Grubka and K. M. Bobba, "Heat transfer characteristics of a continuous, stretching surface with variable temperature," *J. Heat Transfer*, vol. 107, no. 1, pp. 248–250, 1985. DOI: 10.1115/1.3247387.